

NUMERICAL EVALUATION OF SINGLE FIBER MOTION FOR SHORT-FIBER-REINFORCED COMPOSITE MATERIALS PROCESSING

Dongdong Zhang

Department of Mechanical & Aerospace Engineering
University of Missouri, Columbia, MO, USA
dz25c@mail.missouri.edu

Douglas E. Smith

Department of Mechanical & Aerospace Engineering
University of Missouri, Columbia, MO, USA
SmithDoug@missouri.edu

David A. Jack

Department of Mechanical Engineering
Baylor University, Waco, Texas, USA
David_Jack@baylor.edu

Stephen Montgomery-Smith

Department of Mathematics
University of Missouri, Columbia, MO, USA
stephen@missouri.edu

ABSTRACT

This paper presents a computational approach for simulating the motion of a single fiber suspended within a viscous fluid. We develop a Finite Element Method (FEM) for modeling the dynamics of a single rigid fiber suspended in a moving fluid. Our approach seeks solutions using the Newton-Raphson method for the fiber's linear and angular velocities such that the net hydrodynamic forces and torques acting on the fiber are zero. Fiber motion is then computed with a Runge-Kutta method to update the fiber position and orientation as a function of time. Low-Reynolds-number viscous flows are considered since these best represent the flow conditions for a polymer melt within a mold cavity. This approach is first used to verify Jeffery's orbit (1922) and addresses such issues as the role of a fiber's geometry on the dynamics of a single fiber, which were not addressed in Jeffery's original work. The method is quite general and allows for fiber shapes that include, but are not limited to, ellipsoidal fibers (such as that studied in Jeffery's original work), cylindrical fibers and bead-chain fibers. The relationships between equivalent aspect ratio and geometric aspect ratio of cylindrical and other axisymmetric fibers are derived in this paper.

Keywords: Jeffery's orbit, short-fiber-reinforced composite material, fiber orientation, equivalent aspect ratio, cylindrical fiber, axisymmetric fiber

1 INTRODUCTION

Mechanical properties of short-fiber-reinforced composite systems are largely dependent on the fiber orientations within the polymer matrix which are determined during the manufacturing process. The orientation state of the fibers is often computed based on the method first proposed by Jeffery [1], who studied a single ellipsoidal fiber rotating in a Newtonian, incompressible, homogeneous flow. Orientation averaging using Jeffery's approach has since yielded the orientation distribution function [2] and tensor methods [3], which are applied regularly in industrial mold filling simulations. The recent Spherical Harmonic solution approach [4] for solving

Jeffery's equation provides a computationally efficient means to evaluate the previously computationally prohibitive orientation distribution function equations, but is not directly applicable to industrial software solution approaches. Many closure approximations [5,6] have been developed to allow orientation tensor solutions within industrial mold filling software packages, and quickly provide reasonably accurate results.

Jeffery's theory serves as the basis for describing fiber orientations in short-fiber-reinforced composite materials, and better understanding the underlying dependence of the orientation distribution on the fiber's geometry is worth investigating further. Jeffery showed that a single fiber has a closed periodic tumbling motion in simple shear flow, often referred to as the "Jeffery's orbit". Even though this periodic motion has been validated in experiments for dilute suspensions [7-10], the observed period of fiber motion is slower than direct implementations of Jeffery's equation [7]. In addition, the orientation of concentrated fiber suspensions obtained by evaluating orientation tensors in Wang, et.al, [11] shows a deviation from Jeffery's orbit, which may result from the limiting assumptions in Jeffery's original work. Therefore, fiber motion in complicated flows requires us to revisit Jeffery's equation and explore the possible factors that affect fiber motion. In addition, only ellipsoidal fibers were included in Jeffery's theory. However, non-ellipsoidal shapes, such as cylindrical fibers, are of more interest in the area of composites material processing. Therefore, another focus of this paper is to evaluate the motion of cylindrical fibers as well as fibers of other shapes.

Many researchers have extended Jeffery's work to study fiber suspensions in broader areas [12,13]. Jia [14] considered a slip boundary condition on the fiber surface, while Jeffery applied the non-slip boundary condition. Junk [15] theoretically studied the effect of a bounded wall around the fiber, and found that Jeffery's result represents the leading order equation of a singularly perturbed flow problem. Leal [13] analyzed the non-Newtonian effect of a fluid with the presence of fibers, and studied the fiber motion under the consideration of weak fluid inertia. To study non-dilute fiber suspensions, Batchelor [16,17] proposed a constitutive model to take into account the contribution that fibers have on the fluid's total stress tensor. Suspensions of flexible fibers [18-21] have also been simulated. Yamamoto [18] regarded a fiber as a group of beads that are lined up and bonded to each neighbor as a bead chain, referred to as a bead-chain fiber, where each pair of bonded spheres can stretch, bend and twist. Ross and Klingberg [19] and Wang, et al. [20] used a rod-chain model to represent flexible fibers in a similar manner.

One main factor that defines the Jeffery's orbit in a shearing flow is the fiber's geometric aspect ratio, obtained from the fiber's geometry. The study of fibers with different shapes was also considered by Bretherton [22], who proposed that Jeffery's theory is also valid for general axisymmetric bodies with fore-aft symmetry, when an equivalent aspect ratio (r_e^*) is used, instead of geometric aspect ratio (r_e) to quantify the fiber's geometry. For cylindrical fibers, the periodic tumbling motion is observed in [8,10,23,24], but cylindrical fibers have different observed rotation periods from those of ellipsoidal fibers. Trevelyan [8] experimentally estimated the ratio of the equivalent aspect ratio to the geometric aspect ratio (r_e^*/r_e) to be approximately 0.7. Petrich [23] found that the ratio is

0.687 for $r_e = 50$ and 0.623 for $r_e = 72$. Cox [25] proposed a theoretical formula to calculate the equivalent aspect ratio of a slender cylindrical fiber. Unfortunately, his equation is not valid for short rod-like fibers with aspect ratios smaller than 20. Additionally, we note that existing simulation methods have given little attention to other fiber shapes.

With the development of Computational Fluid Dynamics (CFD), the numerical simulation of fiber migration in a viscous fluid has become an effective tool to study fiber orientation [26-29], avoiding difficult or impossible theoretical derivations. Sugihara-Seki [26] evaluated fiber motion in paraboloidal flow using the finite element method, with results that did not quite agree with Chwang's result [27] because of the bounded wall effect. Additionally, this work was limited to planar fiber motion and ignored three-dimensional fiber migration. Feng [28] used Hu's method [29] to simulate fiber motion with two-dimensional finite element simulations. Unfortunately, the two-dimensional problem ignores important three-dimensional flow behavior.

In this paper we present an approach that addresses the general three-dimensional motion of an axisymmetric fiber with various geometries. Specifically, the finite element method is applied to solve the governing equations of fluid flow, so as to evaluate the hydrodynamic forces and torques on a fiber. The Newton-Raphson method is used to search for linear and angular fiber velocities which zero the hydrodynamic forces and torques on the fiber. The Runge-Kutta method updates the fiber position and orientation with respect to time. To ensure the accuracy and robustness of our methodology, the results from our approach are compared with Jeffery's theory using an ellipsoidal fiber.

The remainder of this paper is organized as follows: Section 2 introduces Jeffery's theory and related background information. Section 3 presents the methodology, including the finite element method, the Newton-Raphson iteration method and the Runge-Kutta method. Section 4 presents the computed equivalent aspect ratios of axisymmetric fibers, including ellipsoidal, cylindrical and bead-chain fibers. Implementation and illustrative examples are given in Section 5, and conclusions and future work are presented in Section 6.

2 JEFFERY'S ORBIT

Jeffery [1] first derived the equations of motion for the dynamics of a single ellipsoidal fiber suspended in simple shear flow. In Jeffery's theory, the fiber orientation is defined by three angles (ϕ, θ, ψ) in terms of the global coordinate systems xyz where a local coordinate system $x'y'z'$ translates and rotates with the fiber, as shown in Fig.1. Jeffery assumed that the ellipsoidal fiber's center translates with the same linear velocity as the undisturbed simple shear flow evaluated at fiber centroid.

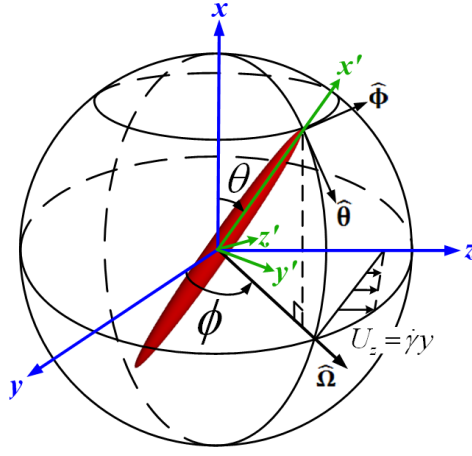


Fig.1 Coordinate systems of a single ellipsoidal fiber in Jeffery's theory: x' axis is along the fiber's semi-long axis, y' axis is defined by rotating vector $\hat{\theta}$ with respect to x' axis by ψ

Applying Lamb's classic treatise [31] and assuming a torque-free particle, Jeffery solved $\phi(t), \theta(t), \psi(t)$ for a simple shear flow with $U_z = \dot{\gamma}y$ (cf. Fig.1) as

$$\phi(t) = \tan^{-1} \left(r_e \tan \frac{\dot{\gamma}t}{r_e + \frac{1}{r_e}} \right) \quad (1)$$

$$\theta(t) = \tan^{-1} \frac{Cr_e}{\sqrt{r_e^2 \cos^2 \phi + \sin^2 \phi}} \quad (2)$$

$$\psi(t) = \int_0^t \left(\frac{\dot{\gamma}}{2} - \dot{\phi} \right) \cos \theta dt \quad (3)$$

where r_e is the geometric aspect ratio of the ellipsoidal fiber (i.e. the ratio of semi-long axis to semi-short axis), and $\dot{\gamma}$ is the shear rate of the undisturbed fluid. The "orbit constant" C is determined by the initial configuration of fiber orientation, and varies between $C = 0$ corresponding to the fiber rolling along its symmetric axis, and $C = +\infty$ which represents the periodic tumbling of fiber in the yz plane, as shown in Fig.2(a). By differentiating Eqs.(1)-(3) with respect to time, expressions for the angular velocities $\dot{\phi}(t), \dot{\theta}(t)$ and $\dot{\psi}(t)$ are obtained. Examples of $\phi(t)$ and $\dot{\phi}(t)$ appear in Fig.2(b) for $C = 1.73$. In Jeffery's theory, a single fiber performs a periodic tumbling motion, with the time period

$$T = \frac{2\pi}{\dot{\gamma}} \left(r_e + \frac{1}{r_e} \right) \quad (4)$$

which is simply a function of the flow shear rate $\dot{\gamma}$ and the ellipsoidal fiber's geometric aspect ratio r_e . Hence, fiber shape has a great influence on the characteristics of fiber migration, which is considered further in Section 4.

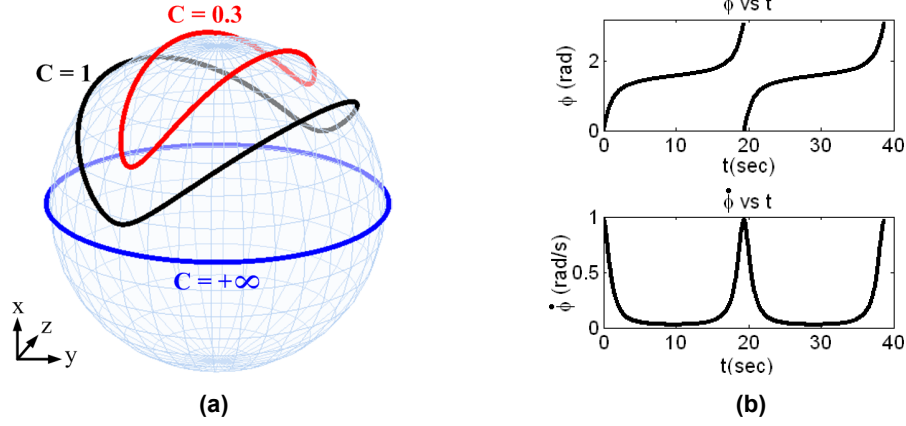


Fig.2 Example calculations of Jeffery's Orbit: (a) Jeffery's orbit with different orbit constants C 's; (b) Values of $\phi(t)$ and $\dot{\phi}(t)$ in one period for $C = 1.73$

3 METHODOLOGY

In this paper, we apply numerical schemes to solve for the motion of a single fiber within a viscous fluid. The basis is that the fiber is migrating with zero net force and torque from the fluid. As in Jeffery's approach, we also use ϕ, θ, ψ to define the fiber's orientation. However, we fix the global coordinate system xyz in space, which is not the same as that in Jeffery's paper, while $x'y'z'$ translates and rotates with the fiber. The position vector of fiber centroid in xyz system is defined as $[x_c, y_c, z_c]^T$, and has a translation velocity $[\dot{x}_c, \dot{y}_c, \dot{z}_c]^T$.

3.1 Fluid Dynamics Simulation

In our approach, the finite element method is used to evaluate the velocity and pressure distribution within a fluid to calculate the forces and torques on a fiber. The governing equations and boundary conditions are defined in the fixed global coordinate system xyz , where the steady Navier-Stokes equation and continuity equation are given respectively as

$$\rho \mathbf{U} \cdot \nabla \mathbf{U} = -\nabla p + \mu \nabla^2 \mathbf{U} \quad (5)$$

$$\nabla \cdot \mathbf{U} = 0 \quad (6)$$

where \mathbf{U} and p are, respectively, the velocity vector and pressure of the fluid, ρ is the density of the fluid, and μ is the absolute viscosity of the fluid. We use tetrahedral meshes to represent the three dimensional fluid domain shown in Fig.3(a), with the two velocity boundaries shown in Fig.3(b): the far-away fluid velocity (BC1) and the fluid velocity on fiber surface (BC2). The velocity boundary conditions are defined as

$$(BC1) \text{ On far-away fluid boundary: } \mathbf{U}_{BC1} = \mathbf{Lx} \quad (7)$$

$$(BC2) \text{ On the fiber surface: } \mathbf{U}_{BC2} = \mathbf{U}_c + B(\boldsymbol{\omega})\mathbf{x} \quad (8)$$

where $\mathbf{U}_C = [\dot{x}_C, \dot{y}_C, \dot{z}_C]^T$ is the translation velocity of the fiber centroid with respect to the coordinate system xyz . On BC1, \mathbf{L} is the velocity gradient of the undisturbed fluid, defined as $\mathbf{L} = \begin{pmatrix} 0 & 0 & 0 \\ 0 & 0 & 0 \\ 0 & \dot{\gamma} & 0 \end{pmatrix}$ for a simple shear flow, where $\dot{\gamma}$ is the uniform shear rate of undisturbed flow. The position vector \mathbf{x} defines a point on fiber surface and $B(\boldsymbol{\omega})$ is the angular velocity matrix, defined as [15]

$$B(\boldsymbol{\omega}) = \dot{\mathbf{R}}\mathbf{R}^T = \begin{bmatrix} 0 & -\omega_z & \omega_y \\ \omega_z & 0 & \omega_x \\ -\omega_y & \omega_x & 0 \end{bmatrix} \quad (9)$$

where $\omega_x, \omega_y, \omega_z$ are the fiber angular velocities with respect to the x, y, z axis, respectively, defined as

$$\boldsymbol{\omega} = \begin{bmatrix} \omega_x \\ \omega_y \\ \omega_z \end{bmatrix} = \begin{bmatrix} \dot{\phi} + \dot{\psi} \cos\theta \\ -\dot{\theta} \sin\phi + \dot{\psi} \sin\theta \cos\phi \\ \dot{\theta} \cos\phi + \dot{\psi} \sin\theta \sin\phi \end{bmatrix} \quad (10)$$

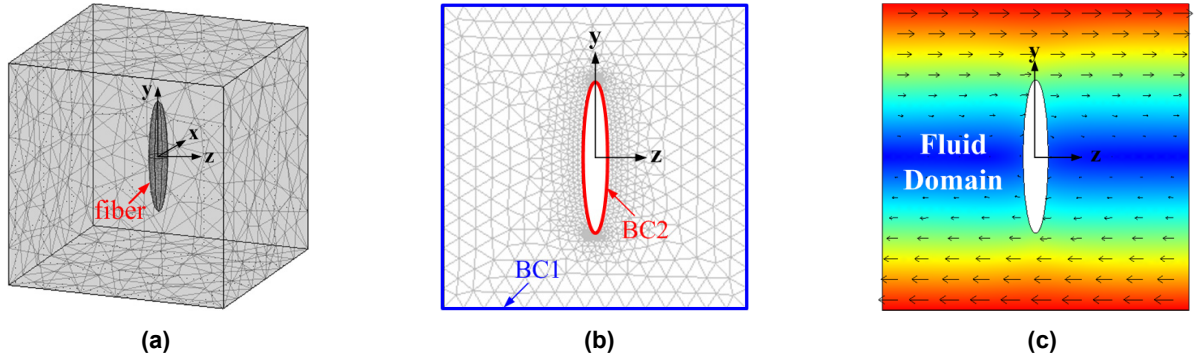


Fig.3 (a) Three-dimensional finite element model; (b) Mesh model in the yz plane with two velocity boundaries; (c) Velocity distribution of fluid domain in the yz plane.

Note that for an axisymmetric fiber, such as an ellipsoid, only ϕ and θ (as shown in Fig.1) are needed to define the fiber's orientation.

For a general, non-axisymmetric fiber, the direction cosine matrix \mathbf{R} (with the time derivative $\dot{\mathbf{R}}$) is required, i.e.,

$$\mathbf{R} = \begin{bmatrix} l_1 & l_2 & l_3 \\ m_1 & m_2 & m_3 \\ n_1 & n_2 & n_3 \end{bmatrix} \quad (11)$$

where

$$\begin{aligned} l_1 &= \cos\theta, & m_1 &= \sin\theta \cos\phi, & n_1 &= \sin\theta \sin\phi \\ l_2 &= -\sin\theta \cos\psi, & m_2 &= -\sin\phi \sin\psi + \cos\theta \cos\phi \cos\psi, & n_2 &= \cos\phi \sin\psi + \cos\theta \sin\phi \cos\psi \\ l_3 &= \sin\theta \sin\psi, & m_3 &= -\sin\phi \cos\psi - \cos\theta \cos\phi \sin\psi, & n_3 &= \cos\phi \cos\psi - \cos\theta \sin\phi \sin\psi \end{aligned}$$

We solve Eqs.(5)-(8) with the finite element method to obtain the net force \mathbf{F} and net torque \mathbf{T} on the fiber computed from the following equations

$$\boldsymbol{\sigma} = -p\boldsymbol{\delta} + \mu[\nabla\mathbf{U} + (\nabla\mathbf{U})^T] \quad (12)$$

$$\mathbf{F} = \int \{\boldsymbol{\sigma} \cdot \mathbf{n}\} dS \quad (13)$$

$$\mathbf{T} = \int \{\mathbf{x} \times (\boldsymbol{\sigma} \cdot \mathbf{n})\} dS \quad (14)$$

In the above, $\boldsymbol{\sigma}$ is the stress in fluid, $\boldsymbol{\delta}$ is the Kronecker delta, dS represents the surface integral, \mathbf{n} is the unit normal vector on fiber surface, $\mathbf{F} = [F_x, F_y, F_z]^T$, and $\mathbf{T} = [T_x, T_y, T_z]^T$.

3.2 Computing Fiber Velocities

In the finite element model, \mathbf{U}_c and $\boldsymbol{\omega}$ define the boundary condition BC2 (cf. Eq.(8)) when solving for \mathbf{U} and p within the fluid, and also the force \mathbf{F} and torque \mathbf{T} from Eq.(13) and Eq.(14), respectively. Therefore, \mathbf{F} and \mathbf{T} are functions of $\dot{x}_c, \dot{y}_c, \dot{z}_c$ and $\dot{\phi}, \dot{\theta}, \dot{\psi}$. The forces and torques exerted on the massless fiber are set to zero (as in Jeffery's original work) at any time t_i as

$$\mathbf{F}(\dot{x}_{ci}, \dot{y}_{ci}, \dot{z}_{ci}, \dot{\phi}_i, \dot{\theta}_i, \dot{\psi}_i) = \mathbf{0} \quad (15)$$

$$\mathbf{T}(\dot{x}_{ci}, \dot{y}_{ci}, \dot{z}_{ci}, \dot{\phi}_i, \dot{\theta}_i, \dot{\psi}_i) = \mathbf{0} \quad (16)$$

using the Newton-Raphson iteration algorithm to compute the fiber's linear and angular velocities at any time t_i . This is done by solving Eq. (15) and Eq.(16) simultaneously as

$$\dot{\mathbf{y}}_{I+1} = \dot{\mathbf{y}}_I - [\mathbf{J}_I]^{-1}[\mathbf{P}_I] \quad (17)$$

Where I is the Newton-Raphson iteration number, $\dot{\mathbf{y}}_I = [\dot{x}_{ci}, \dot{y}_{ci}, \dot{z}_{ci}, \dot{\phi}_i, \dot{\theta}_i, \dot{\psi}_i]^T$, and $[\mathbf{P}_I]$ is a function of \mathbf{F} and \mathbf{T} , given as

$$[\mathbf{P}_I] = [F_x, F_y, F_z, T_x, T_y, T_z]^T \quad (18)$$

In our analysis, $[\mathbf{J}_I]$ is the Jacobian matrix (i.e. the first order partial derivatives of $[\mathbf{P}_I]$ with respect to $\dot{\mathbf{y}}_I$), which is evaluated using the forward finite difference method.

3.3 Evolution of Fiber Motion

At time t_i , we assume that the position of the fiber centroid (x_{ci}, y_{ci}, z_{ci}) and fiber orientation $(\phi_i, \theta_i, \psi_i)$ are given which defines the geometry of the fiber within the finite element simulation. The linear velocities $\dot{x}_{ci}, \dot{y}_{ci}, \dot{z}_{ci}$ and angular velocities $\dot{\phi}_i, \dot{\theta}_i, \dot{\psi}_i$ are then obtained from the converged Newton-Raphson iteration to give $\dot{\mathbf{y}}_i = \mathbf{f}(t_i, \mathbf{y}_i)$, where $\mathbf{y}_i = [x_{ci}, y_{ci}, z_{ci}, \phi_i, \theta_i, \psi_i]^T$. We use a 4th-order

Runge-Kutta algorithm to solve the evolution of $\dot{x}_c, \dot{y}_c, \dot{z}_c, \dot{\phi}, \dot{\theta}, \dot{\psi}$ as a function of time, with the given initial conditions $[x_{c0}, y_{c0}, z_{c0}, \phi_0, \theta_0, \psi_0]$. The algorithm is as follows [32]:

$$\mathbf{y}_{i+1} = \mathbf{y}_i + \frac{1}{6}\Delta t(\mathbf{k}_1 + \mathbf{k}_2 + \mathbf{k}_3 + \mathbf{k}_4) \quad (19)$$

where

$$\mathbf{k}_1 = \mathbf{f}(t_i, \mathbf{y}_i), \quad \mathbf{k}_2 = \mathbf{f}\left(t_i + \frac{1}{2}\Delta t, \mathbf{y}_i + \frac{1}{2}\mathbf{k}_1\Delta t\right), \quad \mathbf{k}_3 = \mathbf{f}\left(t_i + \frac{1}{2}\Delta t, \mathbf{y}_i + \frac{1}{2}\mathbf{k}_2\Delta t\right), \quad \mathbf{k}_4 = \mathbf{f}(t_i + \Delta t, \mathbf{y}_i + \mathbf{k}_3\Delta t)$$

In Eq.(19), Δt represents the time interval in Runge-Kutta method, and \mathbf{y}_{i+1} is the value of \mathbf{y} at time t_{i+1} .

3.4 Summary of Numerical Approach

Our numerical approach proceeds as follows:

STEP 1: At time t_i (i starts from 0), the finite element model for the fluid domain between fiber surface and far-away fluid boundary is defined. In this model, we use $\dot{x}_{ci}, \dot{y}_{ci}, \dot{z}_{ci}$ and $\dot{\phi}_i, \dot{\theta}_i, \dot{\psi}_i$ to define the velocity boundary condition on the fiber surface so as to calculate the hydrodynamic forces and torques exerted on fiber. Note that based on Jeffery's theory, the values of $\dot{x}_{ci}, \dot{y}_{ci}, \dot{z}_{ci}, \dot{\phi}_i, \dot{\theta}_i, \dot{\psi}_i$ will give rise to zero net forces and torques on the fiber.

STEP 2: Use the Newton-Raphson method to calculate the expected $\dot{x}_{ci}, \dot{y}_{ci}, \dot{z}_{ci}, \dot{\phi}_i, \dot{\theta}_i, \dot{\psi}_i$, that generate zero net forces and torques at each time moment t_i . Note that at different time moments, the solutions for the velocities will be different, because the finite element model, defined by $x_{ci}, y_{ci}, z_{ci}, \phi_i, \theta_i, \psi_i$, is changing with respect to time.

STEP 3: Since at any time moment t_i , the linear velocities $\dot{x}_{ci}, \dot{y}_{ci}, \dot{z}_{ci}$ of the fiber centroid and angular velocities $\dot{\phi}_i, \dot{\theta}_i, \dot{\psi}_i$ are obtained, a 4th-order Runge-Kutta algorithm is used to update fiber positions and orientations as functions of time.

4 ROLE OF FIBER SHAPE

The hydrodynamic forces and torques in Eq.(13) and Eq.(14) are evaluated as surface integrals on the exterior of the fiber, thus the fiber shape has a significant effect on the dynamics of fiber motion within a fluid. Jeffery considered an ellipsoid-shaped fiber, but the motion of a fiber with other shapes, such as a cylindrical fiber as would be fabricated from a chopped-fiber process, is of more interest in the field of composites materials processing. Therefore, in this section, we explore the motion of cylindrical fibers and fibers having other axisymmetric shapes.

For any axisymmetric fiber, the geometric aspect ratio r_e is typically defined by the fiber's geometry. For example, r_e of an ellipsoidal fiber is the ratio of the semi-long axis to the semi-short axis. Alternatively, r_e of a cylindrical fiber is commonly defined as the ratio of fiber's length to its diameter. Bretherton [22] theoretically demonstrated that any axisymmetric fiber has periodic tumbling motion,

which is also governed by Jeffery's theory. However, a different aspect ratio, referred to as the equivalent aspect ratio r_e^* is used to quantify the fiber motion instead of the geometric aspect ratio r_e . Cox [25] used the ellipsoidal fiber to derive a formula for the equivalent aspect ratios of other shapes by considering simple shear flow $\mathbf{U} = [0, 0, \dot{\gamma}y]^T$ with an orbit constant $C = +\infty$, such that $\theta = \pi/2, \psi = 0$ and $\dot{\theta} = \dot{\psi} = 0$ in Eq.(10). The resulting angular velocity of the suspended fiber in the coordinate system xyz is

$$\boldsymbol{\omega} = \begin{bmatrix} \omega_x \\ \omega_y \\ \omega_z \end{bmatrix} = \begin{bmatrix} \dot{\phi} \\ 0 \\ 0 \end{bmatrix}$$

where $\dot{\phi}$ is obtained by differentiating Eq.(1) with respect to time as

$$\omega_x = \dot{\phi} = \frac{\dot{\gamma}}{r_e^2 + 1} [1 + (r_e^2 - 1) \cos^2 \phi] \quad (20)$$

Cox considered the angular velocity ω_x when the ellipsoid's long axis is in the vertical direction and the horizontal direction, shown in Fig.4.

In the vertical direction ($\phi = 0$), Eq.(20) yields $[\omega_x]_V = \frac{\dot{\gamma}}{r_e^2 + 1} r_e^2$, and similarly, in the horizontal direction ($\phi = \pi/2$), $[\omega_x]_H = \frac{\dot{\gamma}}{r_e^2 + 1}$.

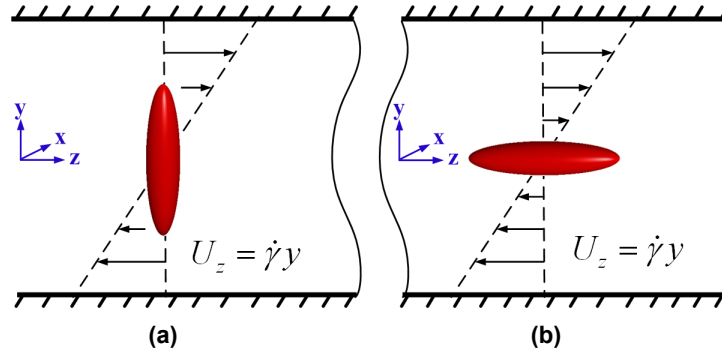


Fig.4 Fiber motion in the yz plane: (a) in the vertical direction ($\phi = 0$); (b) in the horizontal direction ($\phi = \pi/2$)

Therefore, the equivalent aspect ratio of an ellipsoidal fiber is calculated as

$$r_e^* = \sqrt{\frac{[\omega_x]_V}{[\omega_x]_H}} = r_e \quad (21)$$

Note that for an ellipsoidal fiber, the equivalent aspect ratio equals its geometric aspect ratio. Cox [25] proposed that the torque T_x exerted on fibers when the fiber is fixed should be proportional to fiber's angular velocity ω_x when it is free to rotate and translate. Therefore, the equivalent aspect ratio of any axisymmetric fiber is

$$r_e^* = \sqrt{\frac{[\omega_x]_V}{[\omega_x]_H}} = \sqrt{\frac{[T_x]_V}{[T_x]_H}} \quad (22)$$

where $[T_x]_V$ and $[T_x]_H$ represent the torques when the fiber is fixed in the vertical and horizontal directions, respectively. Cox [25] used the slender body theory to calculate the torques in two directions and proposed a closed-form formula, but this formula is only applicable to long cylindrical fibers, not short cylindrical fibers.

In this paper, we use the finite element method to calculate the hydrodynamic torques exerted on fiber in the vertical and horizontal orientations, respectively, with the velocity boundary condition in Eq.(8) as $\mathbf{U}_{BC2} = \mathbf{0}$. In this case, a fiber is fixed within the fluid without translation and rotation, and r_e^* is computed with Eq. (22).

5 IMPLEMENTATION AND EXAMPLES

In this section, several examples are presented to illustrate and validate the proposed approach.

5.1 Validation of Jeffery's orbit

We use our computational methodology to evaluate the motion of a single ellipsoidal fiber in a simple shear flow, and compare with Jeffery's theoretical solution. The problem is set up in Fig. 5, with the parameters tabulated in Table 1, where a and b are the semi-long and semi-short axes of an ellipsoidal fiber, respectively, and H is the distance between the upper and lower boundary of our computational domain and is much larger than the dimension of the fiber to avoid edge effects.

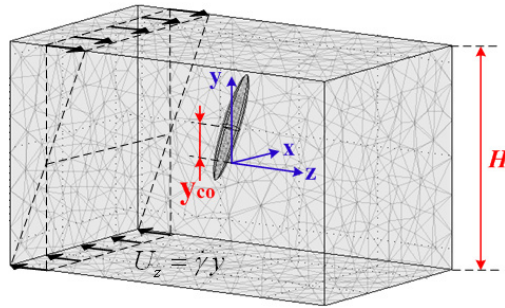


Fig.5 Initial set-up of the motion of a single ellipsoidal fiber in simple shear flow ($U_z = \dot{\gamma}y$)

Table 1. Parameters of ellipsoidal fiber motion	
Parameters	Value
Geometric aspect ratio of ellipsoid	$r_e = \frac{a}{b} = 6$
Undisturbed simple shear flow	$U_z = \dot{\gamma}y$, where $\dot{\gamma} = 1 \text{ sec}^{-1}$
Raito of fiber size to boundary size	$\varepsilon = \frac{2a}{H} = 0.025$
Local particle Reynolds number	$Re \ll 1$
Initial boundary conditions at $t_0 = 0$	$\theta_0 = \pi/3 \text{ (rad)}, \phi_0, \psi_0 = 0 \text{ (rad)}$ $y_{c0} = 0.1 \text{ (mm)}, x_{c0}, z_{c0} = 0 \text{ (mm)}$

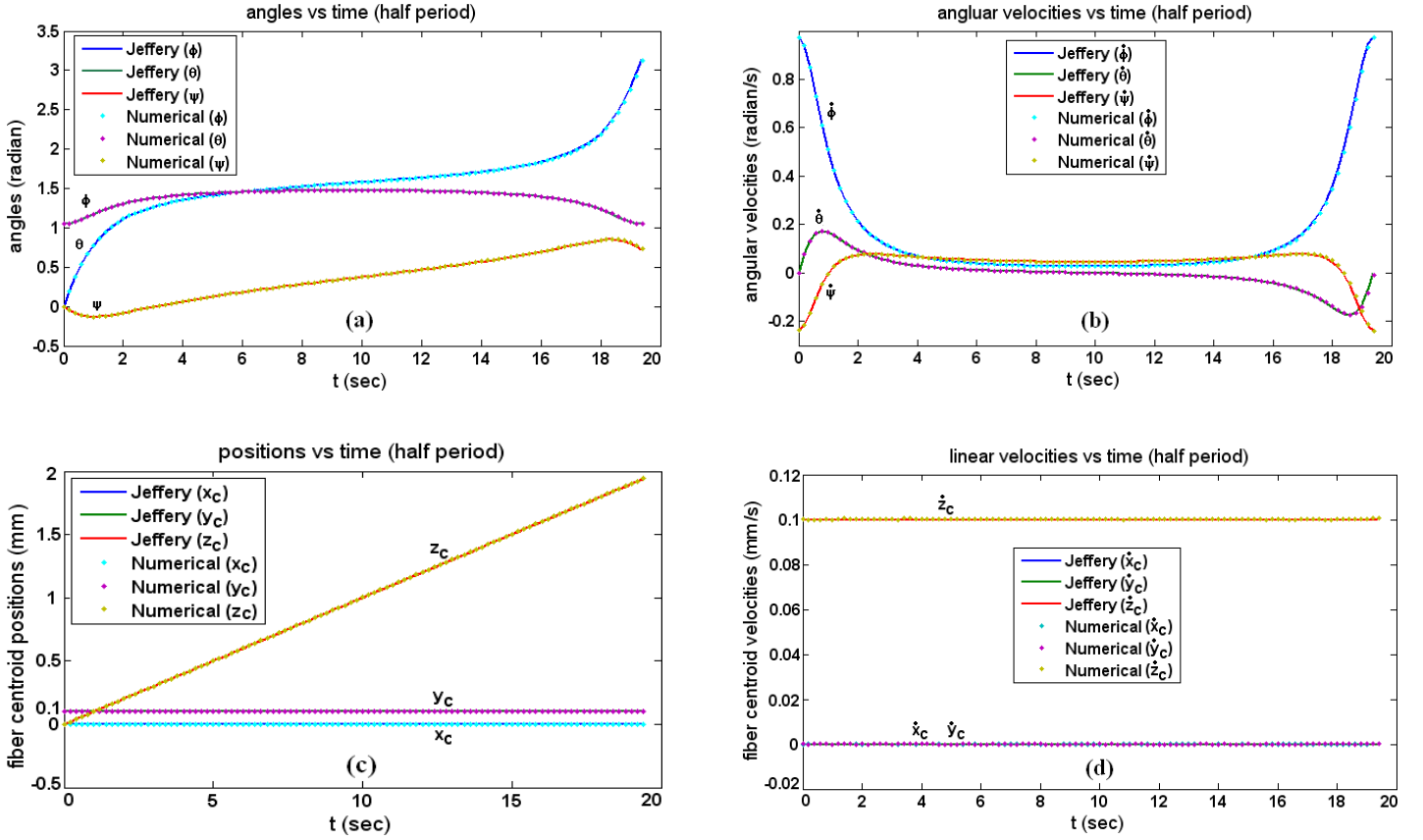


Fig.6 Numerical results of three-dimensional single fiber motion in half period: (a) Evolution of ϕ, θ, ψ ; (b) Evolution of $\dot{\phi}, \dot{\theta}, \dot{\psi}$; (c) Evolution of x_c, y_c, z_c ; (d) Evolution of $\dot{x}_c, \dot{y}_c, \dot{z}_c$

The motion of a single ellipsoidal fiber using our methodology is compared with Jeffery's solution in Fig. 6. In this example, we apply $\Delta t = 0.2$ seconds in the Runge-Kutta method. The initial y_{c0} equals $0.1mm$, so the initial linear velocity of fiber center in the z direction is $\dot{z}_{c0} = \dot{\gamma}y_{c0} = 0.1mm/s$. Fig.6(a) and Fig.6(b) show that the fiber orientation agrees with Jeffery's equation and Fig. 6(c) and Fig. 6(d) illustrate that the fiber centroid translates with the same linear velocity as the undisturbed fluid evaluated at fiber's centroid. The comparison of two sets of data, i.e. Jeffery's data and our numerical data appear in Table 2, where the mean and standard deviation of the absolute errors are computed over N time steps as

$$Mean = \frac{1}{N} \sum_{i=1}^N |A_i - B_i| \quad (23)$$

$$Std = \sqrt{\frac{1}{N-1} \sum_{i=1}^N (|A_i - B_i| - Mean)^2} \quad (24)$$

where A_i and B_i are, respectively, Jeffery's data and our numerical data in each time step t_i . Note that A and B represent any of the angular velocities or linear velocities.

Table 2. Comparison of data between Jeffery's theory and our approach		
Data Sets	Mean of Absolute Errors	Std. of Absolute Errors
ϕ (radians)	7.2E-5	15.6E-5
θ (radians)	1.6E-5	2.8E-5
φ (radians)	3.5E-5	4.7E-5
x_c (mm)	6E-5	2.5E-5
y_c (mm)	17E-5	8.3E-5
z_c (mm)	0.0016	0.001

Note that in order to verify Jeffery's orbit, we maintain the following conditions within our finite element model, which are analogous to Jeffery's assumptions:

a) The flow domain is much larger than the fiber's dimension. Jeffery assumed the unbounded fluid domain in his paper, so we set $\varepsilon = 2a/H = 0.025$, which provides a good agreement with Jeffery's results. And our simulations show that when $\varepsilon < 0.05$, the results are stable.

b) The local particle Reynolds number $Re = \rho U(2a)/\mu$ is much smaller than 1, where ρ is the fluid density, μ is the absolute viscosity of fluid, U represents the characteristic velocity and $2a$ is the characteristic length of fiber. Therefore, the inertial terms $\left(\rho \frac{\partial \mathbf{U}}{\partial t} + \mathbf{U} \cdot \nabla \mathbf{U}\right)$ can be neglected in Navier-Stokes equation, which is consistent with Jeffery's theory.

The excellent agreement between Jeffery's theory and our approach validate the accuracy and robustness of our approach. More importantly, our approach is a systematic methodology which may be extended to fibers with different shapes and in other flow conditions, which were not addressed in Jeffery's original work.

5.2 Equivalent aspect ratio – General axisymmetric fibers

In this section, we consider the motion of other axisymmetric fibers, and numerically determine the equivalent aspect ratios of axisymmetric fibers, including ellipsoidal, cylindrical, and bead-chain fibers over a large range of aspect ratios.

A) Ellipsoidal fibers The concept of equivalent aspect ratio is proposed based on the analysis of an ellipsoidal fiber, seen from Eqs.(21)(22). Therefore, the equivalent aspect ratio of an ellipsoidal fiber is expected to be the same as the geometric aspect ratio, which is validated by our numerical data tabulated in Table 3.

Table 3. Equivalent aspect ratios of ellipsoidal fiber		
Geometric Aspect ratio (r_e)	Equivalent Aspect ratio (r_e^*)	Relative True Error
1	1.01	0.01
5	5.01	0.0016
10	9.91	0.009
15	14.85	0.01
20	20.15	0.007
30	30.00	3.9E-5
40	39.60	0.01
50	49.90	0.002

B) Cylindrical fibers For a cylindrical fiber, the geometric aspect ratio is defined as the ratio of the length (L) to the diameter (d), shown in Fig.7, where the equivalent aspect ratio of a cylinder is calculated with Eq.(22), and the torques are evaluated using our numerical method.

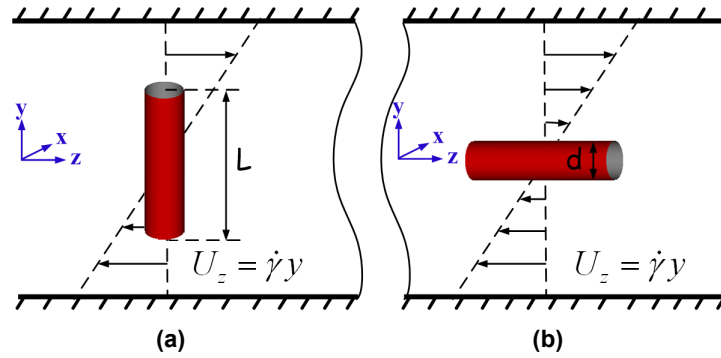


Fig.7 (a) Fiber fixed in the vertical direction; (b) Fiber fixed in the horizontal direction

The relationship between the equivalent aspect ratio r_e^* and geometric aspect ratio r_e is shown in Fig.8. For cylindrical fibers, we plot our numerical data with that from Cox's theoretical equation [25] and experimental data from [8-10,23,33]. Cox [25] used slender body theory to calculate the torques so as to obtain the equivalent aspect ratios of cylinders from Eq.(20), with the expression

$$r_e^* = r_e 1.24 / \sqrt{\ln(r_e)} \quad (25)$$

However, Eq.(25) is only applicable to long rod-like fibers, not short cylindrical fibers due to the end-effects of the fluid on the fiber. Therefore, this formula is ineffective for fibers used in short-fiber-reinforced composite materials.

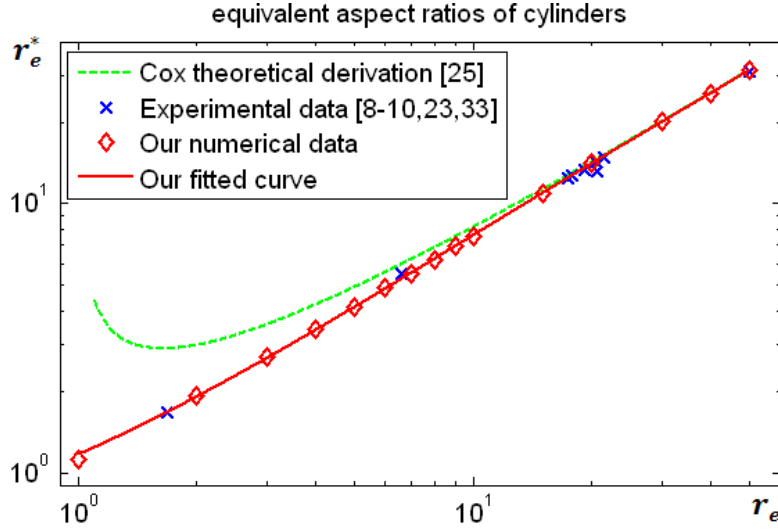


Fig.8 Comparison of our numerical data (red diamonds) and fitted curve (red line) with Cox's theoretical curve (dashed green curve) for slender fibers and experimental data (blue crosses)

From Fig.8 we can see that for long fibers, our data matches well with Cox's theory and conforms to the experimental data [8-10,23,33]. We use a cubic polynomial to fit our numerical data in Fig.8, so as to obtain the closed-form expression

$$r_e^* = 0.000035r_e^3 - 0.00467r_e^2 + 0.764r_e + 0.404 \quad (26)$$

with the fitting correlation coefficient 0.99998. Equation (26) is applicable to both short and long cylindrical fibers with the geometric aspect ratios from 1 to 50.

C) Bead-chain fibers Bead-chain fibers are commonly used to model flexible fibers. Hence, the study of equivalent aspect ratios of bead-chain fibers will provide insight into the study of flexible fibers motion. For a bead-chain fiber, the geometric aspect ratio is defined as the number of beads connected together. For instance, the geometric aspect ratio is 4 in Fig.9. We numerically obtained the torques when the fiber is fixed as shown in Fig.9 using the computational approach described above.

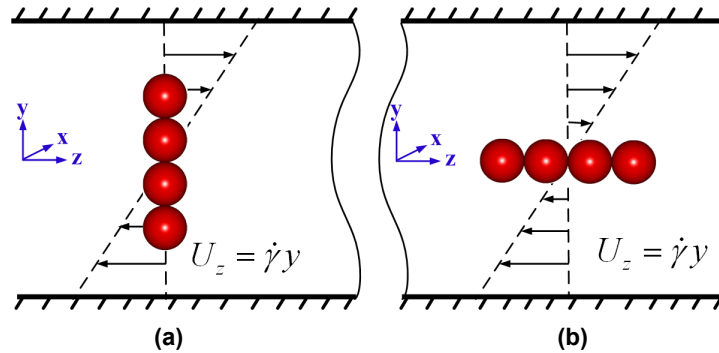


Fig.9 (a) Fiber fixed in the vertical direction ($\phi = 0$); (b) Fiber fixed in the horizontal direction ($\phi = \pi/2$)

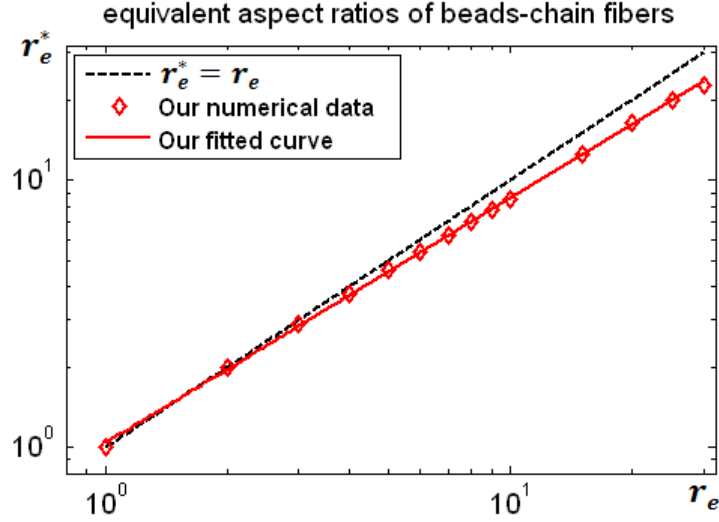


Fig.10 Equivalent aspect ratios of bead-chain fibers: red diamonds represent our numerical data and red line is our fitted curve of the data.

Eq.(22) is used to obtain the numerical data of equivalent aspect ratios of bead-chain fibers, shown in Fig.10. From Fig.10, we see that the equivalent aspect ratio of a bead-chain fiber is different from its geometric aspect ratio. As the fiber gets longer, the difference becomes larger. By fitting our numerical data in Fig.10, we propose the following fitted formula to calculate the equivalent aspect ratios:

$$r_e^* = -0.005r_e^2 + 0.902r_e + 0.145 \quad (27)$$

with the fitting correlation coefficient 0.99965. Note that for our fitted data, the geometric aspect ratios are from 1 to 30.

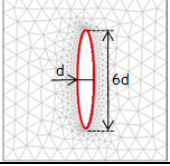
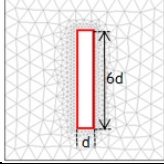
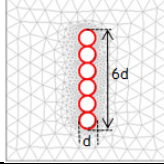
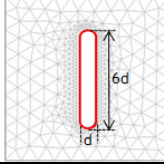
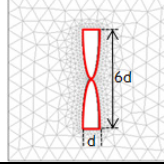
We notice that in current research [18] on flexible fibers using the bead-chain model, the forces and torques on the fiber are calculated based on each separate sphere independently, i.e. when calculating the force and torque on the top sphere, it is assumed that there are no other connecting spheres around the top sphere within the fluid. This assumption is not valid in reality, due to the flow shielding from the neighboring sphere causing changes in the local velocity profile of the fluid, which in turn will change the force and torque distribution on the exterior surface of the top sphere. Accounting for the flow shielding should better represent the physical system the bead-chain models approximate. The results from our study for the equivalent aspect ratios of bead-chain fibers are provided in Table 4 for both scenarios, with and without flow shielding.

Table 4. Comparison of two bead-chain models		
Geometric Aspect ratio (r_e)	Including Beads (r_e^*)	Isolated Beads (r_e^*)
2	2.0	1.6
4	3.7	3.0

6	5.4	4.4
8	7.0	5.8
10	8.6	7.2

From Table 4, we see that assuming isolated beads does not reflect the real equivalent aspect ratios of bead-chain fibers.

D) Comparison of equivalent aspect ratios We summarize the equivalent aspect ratios of various axisymmetric fibers, all having a geometric aspect ratio $r_e = 6$, as shown in Table 5.

Table 5. Comparison of equivalent aspect ratios					
Fiber Shapes	Ellipsoid	Cylinder	Bead-chain	Cylinder with round ends	Two half ellipsoids
FEM in 2D Cross Section					
r_e	$r_e = 6$	$r_e = 6$	$r_e = 6$	$r_e = 6$	$r_e = 6$
r_e^*	$r_e^* = 6$	$r_e^* = 4.8$	$r_e^* = 5.4$	$r_e^* = 5.1$	$r_e^* = 5.2$

Note that even though the geometric aspect ratios of different fibers are the same, the equivalent aspect ratios are quite distinct, resulting in the different fiber motions.

5.3 Validation of equivalent aspect ratio

In this section, we use the methodology, proposed in Section 3 to solve the motion of a cylindrical fiber and a bead-chain fiber, so as to validate our numerical data for equivalent aspect ratios.

A) Cylindrical fibers In this example we consider $r_e = 6$ for a cylindrical fiber. The shear rate of the undisturbed simple shear flow is $1s^{-1}$, and the initial conditions are $\theta_0 = \pi/3 (rad)$, $\phi_0 = \psi_0 = 0 (rad)$ and $x_0 = y_0 = z_0 = 0(mm)$. The evolution of ϕ, θ, φ and $\dot{\phi}, \dot{\theta}, \dot{\varphi}$ are shown in Fig.11, in which the orientation of a cylindrical fiber is obtained using the methodology proposed in Section 3, while the orientation of an ellipsoidal fiber is evaluated from Jeffery's analytical formula.

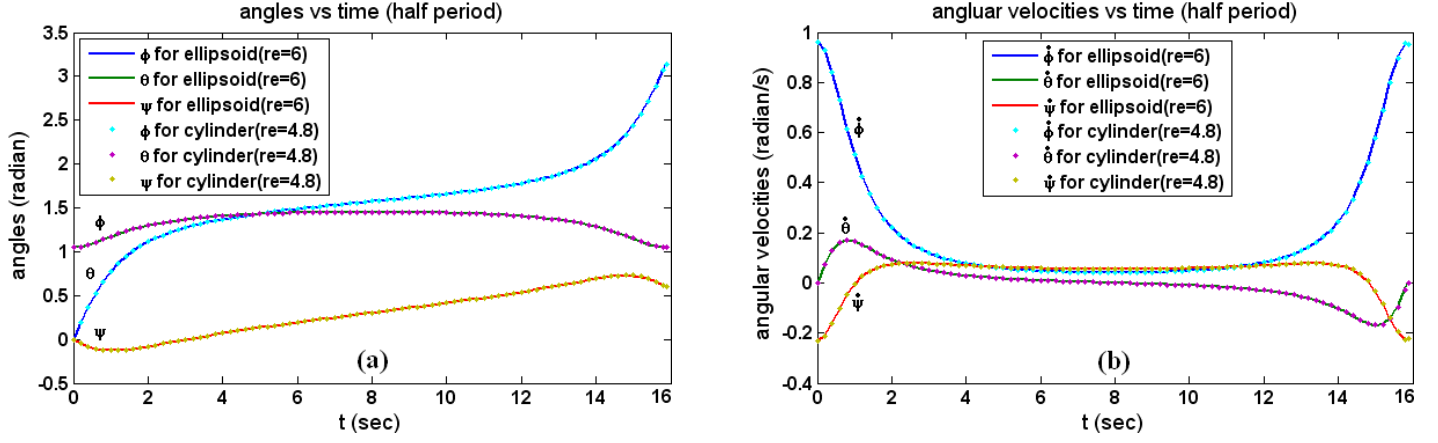


Fig.11 Evolution of a cylindrical fiber with geometric aspect ratio $r_e = 6$ and an ellipsoidal fiber with $r_e = 4.8$: (a) Evolution of ϕ, θ, ψ ; (b) Evolution of $\dot{\phi}, \dot{\theta}, \dot{\psi}$

Fig.11 shows that a cylinder with $r_e = 6$ has the same rotation as that of an ellipsoid with $r_e = 4.8$, i.e. the equivalent aspect ratio of a cylinder with $r_e = 6$ is 4.8. Therefore, the equivalent aspect ratios obtained using our computations with Eq.(22) are validated.

B) Bead-chain fibers Similarly, we evaluate the motion of a bead-chain fiber with $r_e = 6$. The shear rate of the undisturbed simple shear flow is $1s^{-1}$, and the initial conditions are $\theta_0 = \pi/3$ (rad), $\phi_0 = \psi_0 = 0$ (rad) and $x_0 = y_0 = z_0 = 0$ (mm). The results are shown in Fig.12, in which the motion of a bead-chain fiber is evaluated by our numerical schemes while the motion of an ellipsoidal fiber is obtained from Jeffery's analytical solution.

From Fig.12, we can see the bead-chain fiber with the geometric aspect ratio $r_e = 6$ has the same rotational movement as that of the ellipsoidal fiber with $r_e = 5.4$, which validates our numerical data for equivalent aspect ratios of bead-chain fibers.

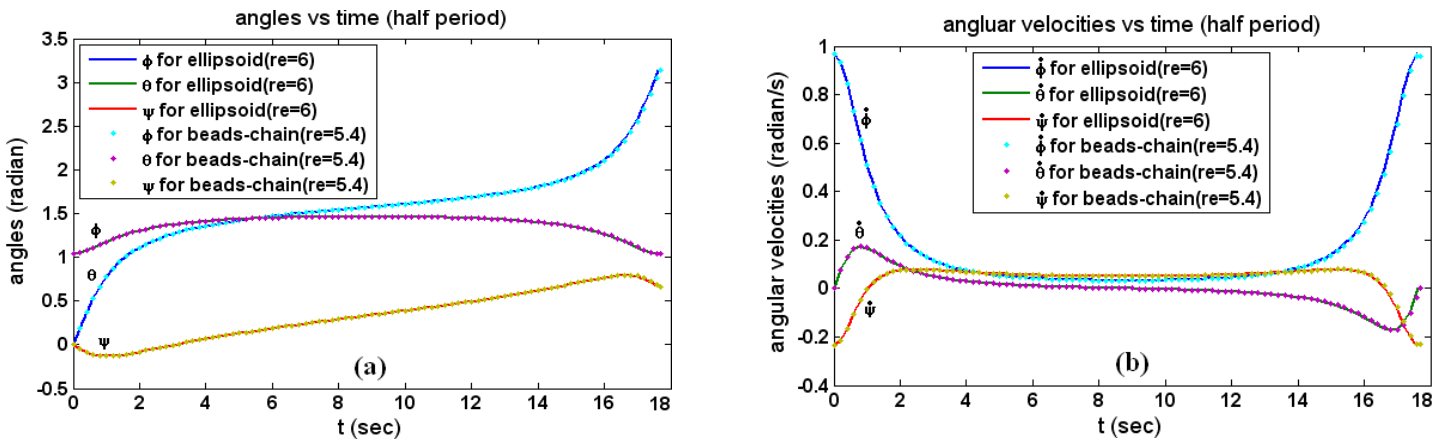


Fig.12 Evolution of a bead-chain fiber with the geometric aspect ratio $r_e = 6$ and an ellipsoidal fiber with $r_e = 5.4$: (a) Evolution of ϕ, θ, ψ ; (b) Evolution of $\dot{\phi}, \dot{\theta}, \dot{\psi}$.

C) Comparison of the motions of different shapes With the same geometric aspect ratio $r_e = 6$, ellipsoidal fiber, cylindrical fiber and bead-chain fiber have different motions, compared in Fig.13.

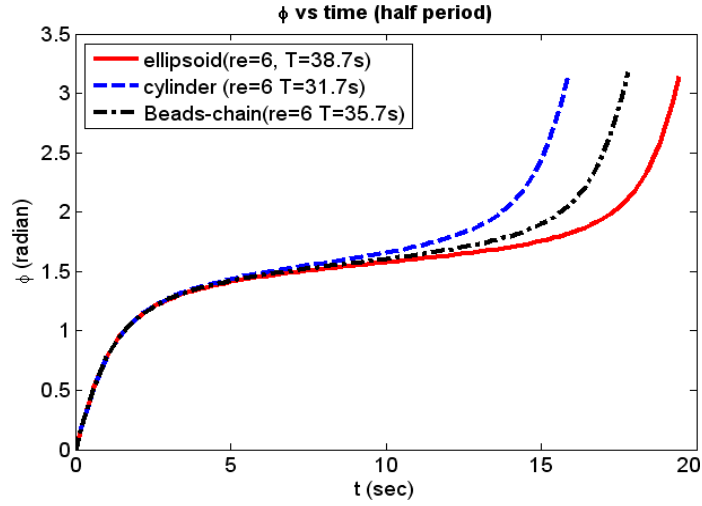


Fig.13 Comparison of the motions of ellipsoid, cylinder and bead-chain fiber with the same geometric aspect ratio $r_e = 6$ (period T given as shown)

We can see that an ellipsoid has the longest period compared with the cylindrical fiber and bead-chain fiber. Note that the cylindrical fiber has the shortest period among these three shapes, such that we would expect the cylinder to move quickly align with the flow than the other shapes.

6 CONCLUSIONS AND FUTURE WORK

A methodology, which combines the finite element method, a Newton-Raphson iteration and a Runge-Kutta method, is presented to solve the general three-dimensional motion of a single suspended fiber within a viscous fluid. This method is very general and can be applied to any axisymmetric fiber, and in the present study results were presented for ellipsoidal, cylindrical and bead-chain fibers.

We demonstrate that the fiber's shape has a significant impact on the fiber orientation direction vector, which will affect the rate of fiber alignment in a short-fiber-reinforced composite material. For an axisymmetric fiber, the equivalent aspect ratio is needed for numerical solutions of the Jeffery's equation for fiber motion instead of the geometric aspect ratio. The equivalent aspect ratios of cylindrical fibers and other fiber types are generated using our finite element method, and are validated by evaluating the fiber motion numerically.

Future work could extend this methodology to fiber motion in various complex fluids, such as Poiseuille flow and a non-Newtonian flow. Another exciting work is to use the proposed method to study the motion of nano-particles.

ACKNOWLEDGEMENTS

The financial support from the National Science Foundation through CMMI-MPM (NSF grant #0727399) is gratefully acknowledged.

REFERENCES

- [1] Jeffery, G. B., 1922, "The Motion of Ellipsoidal Particles Immersed in a Viscous Fluid", Proc. Roy. Soc. London. Series A, Containing Papers of a Mathematical and Physical Character, Vol. 102, Iss. 715, pp. 161-179.
- [2] Folgar F. and Tucker III, C. L., 1984, "Orientation Behavior of Fibers in Concentrated Suspensions", Journal of Reinforced Plastics and Composites, Vol. 3, Iss. 2, pp. 98-119.
- [3] Advani, S. G. and Tucker III, C. L., 1987, "The Use of Tensors to Describe and Predict Fiber Orientation in Short Fiber Composites", Journal of Rheology, Vol. 31, Iss.8, pp. 751-784.
- [4] Montgomery-Smith, Stephen, Jack, D. A. and Smith, D. E., 2011, "The Fast Exact Closure for Jeffery's Equation with Diffusion", Journal of Non-Newtonian Fluid Mechanics, to appear.
- [5] Cintra, J. S. and Tucker III, C. L., 1995, "Orthotropic Closure Approximations for Flow-induced Fiber Orientation", Journal of Rheology, Vol. 39, Iss. 6, pp. 1095-1122.
- [6] Jack, D. A. and Smith, D. E., 2005, "An Invariant Based Fitted Closure of the Sixth-order Orientation Tensor for Short-fiber Suspensions", Journal of Rheology, Vol. 49, Iss. 5, pp.1091-1115.
- [7] Taylor, G. I., 1923, "The Motion of Ellipsoidal Particles in a Viscous Fluid", Proc. Roy. Soc. London. Series A, Containing Papers of a Mathematical and Physical Character, Vol. 103, No. 720, pp. 58-61.
- [8] Trevelyan, B. J. and Mason, S.G., 1951, "Particle Motions in Sheared Suspensions. I. Rotations," Journal of Colloid Science, Vol. 6, pp. 354-367.
- [9] Mason, S. G. and Manley, R. S. J., 1956, "Particle Motions in Sheared Suspensions: Orientation and Interactions of Rigid Rods", Proc. Roy. Soc. London, Vol. 238, No. 1212, pp.117-131.
- [10] Anczurowski, E. and Mason, S. G., 1968, "Particle Motions in Sheared Suspensions. XXIV. Rotation of Rigid Spheroids and Cylinders", Transactions of the Society of Rheology, Vol. 12, Iss. 2, pp. 209-215.
- [11] Wang, J., O'Gara, J. F. and Tucker III, C. L., 2008, "An Objective Model for Slow Orientation Kinetics in Concentrated Fiber Suspensions: Theory and Rheological Evidence", Vol. 52, Iss. 5, pp. 1179-1200.
- [12] Christopher, J. S. Petrie, 1999, "The Rheology of Fiber Suspensions", Journal of Non-Newtonian Fluid Mechanics, Vol. 87, Iss. 2-3, pp. 369-402.
- [13] Leal, L. G., 1980, "Particle Motions in a Viscous Fluid", Annual Review of Fluid Mechanics, Vol. 12, Iss. 1, pp. 435-476.
- [14] Jia, L., 2006, "Flow-induced Alignment Migration of Particles in Suspensions", Ph.D. thesis, Michigan State University.

- [15] Junk, M. and Illner, R., 2007, "A New Derivation of Jeffery's Equation", *Journal of Mathematical Fluid Mechanics*, Vol. 9, No. 4, pp. 445-288.
- [16] Batchelor, G. K., 1970, "The Stress System in a Suspension of Force-free Particles", *Journal of Fluid Mechanics*, Vol.41, pp. 545-570.
- [17] Batchelor, G. K., 1970, "Slender Body Theory for Particles of Arbitrary Cross-section in Stoke Flow", *Journal of Fluid Mechanics*, Vol. 44, pp. 419-440.
- [18] Yamamoto, S. and Matsuoka, T., 1993, "A Method for Dynamic Simulation of Rigid and Flexible Fibers in a Flow Field", *Journal of Chemical Physics*, Vol. 98, Iss. 1, pp.644-650.
- [19] Ross, R. F. and Klingenberg, D. J., 1997, "Dynamic Simulation of Flexible Fibers Composed of Linked Rigid Bodies", *Journal Of Chemical Physics*, Vol.106, Iss.7, pp. 2949-2960.
- [20] Wang, G., Yu, W., and Zhou, C., 2006, "Optimization of the Rod Chain Model to Simulate the Motions of a Long Flexible Fiber in Simple Shear Flows", *European Journal of Mechanics - B/Fluids*, Vol. 25, Iss. 3, pp. 337-347.
- [21] Switzer III, L. H., 2002, "Simulating Systems of Flexible Fibers", Ph.D. thesis, University of Wisconsin-Madison.
- [22] Bretherton, F. P., 1962, "The Motion of Rigid Particles in a Shear Flow at Low Reynolds Number", *Journal of Fluid Mechanics*, Vol.14, Iss. 2, pp. 284-304.
- [23] Petrich, M. P., Koch, D. L.& Cohen C., 2000, "An Experimental Determination of the Stress-microstructure Relationship in Semi-concentrated Fiber Suspension", *Journal of Non-Newtonian Fluid Mechanics*, Vol. 95, Iss. 2-3, pp.101-133.
- [24] Harris, J. B. and Pittman, J. F. T., 1975, "Equivalent Ellipsoidal Aspect Ratios of Slender Rod-like Particles", *Journal of Colloid and Interface Science*, Vol. 50, No. 2, PP. 280-282.
- [25] Cox, R. G., 1971, "The Motion of Long Slender Bodies in a Viscous Fluid. Part2. Shear Flow", *Journal of Fluid Mechanics*, Vol. 45, part 4, pp.625-657.
- [26] Sugihara-Seki, M. 1996, "The Motion of an Ellipsoid in Tube Flow at Low Reynolds Numbers", *Journal of Fluid Mechanics*, Vol. 324, pp. 287-308.
- [27] Chwang, A. T., 1975, "Hydromechanics of Low-Reynolds-Number Flow. Part3. Motion of a Spheroidal Particle in Quadratic Flows", *Journal of Fluid Mechanics*, Vol. 72, Part 1, pp. 17-34.
- [28] Feng, J., Hu, H. H., and Joseph, D. D., 1994, "Direction Simulation of Initial Value Problems for the Motion of Solid Bodies in a Newtonian Fluid, Part2. Couette and Poiseuille Flows", *Journal of Fluid Mechanics*, Vol. 277, pp. 271-301.

- [29] Hu, H. H., Joseph, D. D. and Crochet, M. J., 1992, "Direct Simulation of Fluid Particle Motions", Theoretical and Computational Fluid Dynamics, Vol. 3, pp. 285-306.
- [30] Kittipoomwong, P., See, H. and Mai-Duy, N., 2010, "Dynamic Simulation of Non-spherical Particulate Suspensions", Rheologica Acta, Vol. 49, No. 6, pp. 597-606.
- [31] Lamb, H., 1916, "Hydrodynamics", Cambridge university press.
- [32] Chapra, S. C., 2008, "Applied Numerical Methods with MATLAB for Engineers and Scientists-Second Edition", McGraw-Hill.
- [33] Chaffey, C. E., Takano, M. and Mason, S. G., 1965, "Particle Motions in Sheared Suspensions. XVI. Orientations of Rods and Disks in Hyperbolic and Other Flows", Canadian Journal of Physics, Vol.43, pp. 1269-1287.

Listing of figure and table captions:

Figures:

Fig.1 Coordinate systems of a single ellipsoidal fiber in Jeffery's theory: x' axis is along the fiber's semi-long axis, y' axis is defined by rotating vector $\hat{\theta}$ with respect to x' axis by ψ

Fig.2 Example calculations of Jeffery's Orbit: (a) Jeffery's orbit with different orbit constants C 's; (b) Values of $\phi(t)$ and $\dot{\phi}(t)$ in one period for $C = 1.73$

Fig.3 (a) Three-dimensional finite element model; (b) Mesh model in the yz plane with two velocity boundaries; (c) Velocity distribution of fluid domain in the yz plane.

Fig.4 Fiber motion in the yz plane: (a) in the vertical direction ($\phi = 0$); (b) in the horizontal direction ($\phi = \pi/2$)

Fig.5 Initial set-up of the motion of a single ellipsoidal fiber in simple shear flow ($U_z = \dot{\gamma}y$)

Fig.6 Numerical results of three-dimensional single fiber motion in half period: (a) Evolution of ϕ, θ, φ ; (b) Evolution of $\dot{\phi}, \dot{\theta}, \dot{\varphi}$; (c) Evolution of x_c, y_c, z_c ; (d) Evolution of $\dot{x}_c, \dot{y}_c, \dot{z}_c$

Fig.7 (a) Fiber fixed in the vertical direction; (b) Fiber fixed in the horizontal direction

Fig.8 Comparison of our numerical data (red diamonds) with Cox's theoretical curve (dashed green curve) for slender fibers and experimental data (blue crosses)

Fig.9 (a) Fiber fixed in the vertical direction ($\phi = 0$); (b) Fiber fixed in the horizontal direction ($\phi = \pi/2$)

Fig.10 Equivalent aspect ratios of bead-chain fibers

Fig.11 Evolution of a cylindrical fiber with geometric aspect ratio $r_e = 6$ and an ellipsoidal fiber with $r_e = 4.8$: (a) Evolution of ϕ, θ, φ ; (b) Evolution of $\dot{\phi}, \dot{\theta}, \dot{\varphi}$

Fig.12 Evolution of a bead-chain fiber with the geometric aspect ratio $r_e = 6$ and an ellipsoidal fiber with $r_e = 5.4$: (a) Evolution of ϕ, θ, φ ; (b) Evolution of $\dot{\phi}, \dot{\theta}, \dot{\varphi}$.

Fig.13 Comparison of the motions of ellipsoid, cylinder and bead-chain fiber with the same geometric aspect ratio $r_e = 6$ (period T given as shown)

Tables:

Table 1. Parameters of ellipsoidal fiber motion

Table 2. Comparison of data between Jeffery's theory and our approach

Table 3. Equivalent aspect ratios of ellipsoidal fiber

Table 4. Comparison of two bead-chain models

Table 5. Comparison of equivalent aspect ratios